Journal of Structural Biology: X 4 (2020) 100017

Contents lists available at ScienceDirect

Journal of Structural Biology: X

journal homepage: www.journals.elsevier.com/journal-of-structural-biology-x

Small angle X-ray scattering and molecular dynamic simulations provide molecular insight for stability of recombinant human transferrin

Alina Kulakova[a], Sowmya Indrakumar[a], Pernille Sønderby[a], Lorenzo Gentiluomo[b,c], Werner Streicher[d], Dierk Roessner[b], Wolfgang Frieß[c], Günther H.J. Peters[a], Pernille Harris[a,*]

[a] Department of Chemistry, Technical University of Denmark, Kemitorvet 207, 2800 Kgs. Lyngby, Denmark
[b] Wyatt Technology Europe GmbH, Hochstrasse 18, 56307 Dernbach, Germany
[c] Department of Pharmacy, Pharmaceutical Technology and Biopharmaceutics, Ludwig-Maximilians-University of Munich, Butenandtstrasse 5, 81377 Munich, Germany
[d] Novozymes A/S, Biologiens Vej 2, 2800 Kgs. Lyngby, Denmark

ARTICLE INFO

Keywords:
transferrin
stability
formulation
small angle X-ray scattering
molecular dynamics

ABSTRACT

Transferrin is an attractive candidate for drug delivery due to its ability to cross the blood brain barrier. However, in order to be able to use it for therapeutic purposes, it is important to investigate how its stability depends on different formulation conditions. Combining high-throughput thermal and chemical denaturation studies with small angle X-ray scattering (SAXS) and molecular dynamics (MD) simulations, it was possible to connect the stability of transferrin with its conformational changes. Lowering pH induces opening of the transferrin N-lobe, which results in a negative effect on the stability. Presence of NaCl or arginine at low pH enhances the opening and has a negative impact on the overall protein stability.

Statement of Significance: Protein-based therapeutics have become an essential part of medical treatment. They are highly specific, have high affinity and fewer off-target effects. However, stabilization of proteins is critical, time-consuming, and expensive, and it is not yet possible to predict the behavior of proteins under different conditions. The current work is focused on a molecular understanding of the stability of human serum transferrin; a protein which is abundant in blood serum, may pass the blood brain barrier and therefore with high potential in drug delivery. Combination of high throughput unfolding techniques and structural studies, using small angle X-ray scattering and molecular dynamic simulations, allows us to understand the behavior of transferrin on a molecular level.

1. Introduction

Over the last decades, the number of approved protein-based therapeutics has increased significantly and these drugs have become essential for the treatment of various diseases, such as diabetes, hemophilia, hepatitis C, and cancer (Wishart et al., 2006). This is because, compared to small molecules, protein-based therapeutics show higher specificity and therefore, generally, have less side effects. However, due to their high complexity, protein-drugs are less stable and require special conditions (formulations) that will preserve their stability during production and storage. Under inappropriate conditions, proteins have a high tendency to unfold, which may lead not only to a loss of activity, but also to aggregation (Wang, 1999). Unfortunately, no general rules for formulation have been reported, because it is not yet possible to predict the behavior of different proteins under different conditions. Therefore, it is important to obain a detailed molecular understanding of the rationale behind protein stability and conformational changes.

Typically the protein-drugs cannot cross the blood brain barrier (BBB), which is essential for treatment of certain diseases, such as Alzheimer's disease and brain cancer. One of the strategies to overcome this problem is to attach protein-drugs to a protein that is able to cross the BBB. Therefore, transferrin is an attractive candidate for drug delivery (Shen et al., 2019; Wang et al., 2006; Yoon et al., 2018), since it is one of the most abundant and stable proteins in human plasma (Porter et al., 2006), and it is able to cross the BBB through receptor-mediated endocytosis (Fishman et al., 1987).

Human serum transferrin (TrF) is a major iron-carrying protein in the blood. TrF regulates iron levels in biological fluids, and not only supplies the cells with ferric iron, but also prevents production of radicals in the blood by removing free iron (de Jong et al., 1990). TrF is a multidomain protein, which is composed of two similar lobes: the N-

* Corresponding author.
E-mail address: ph@kemi.dtu.dk (P. Harris).

https://doi.org/10.1016/j.yjsbx.2019.100017
Received 12 September 2019; Received in revised form 15 November 2019; Accepted 25 November 2019
Available online 30 November 2019

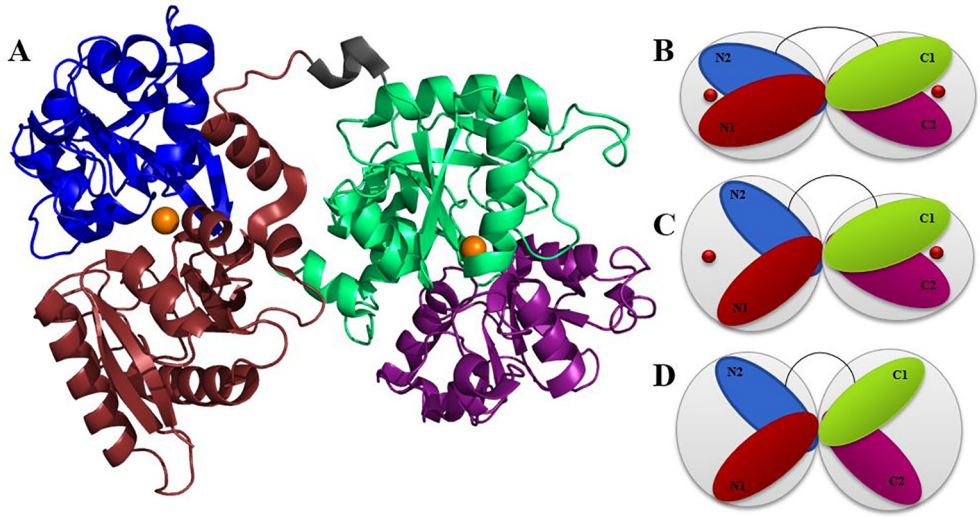

Fig. 1. A: Crystal structure of the closed conformation of TrF (pdbid: 3V83) (Noinaj et al., 2012) and conformational representations for B: closed, C: partially open, and D: fully open conformations. (For interpretation of the references to colour in this figure legend, the reader is referred to the web version of this article.)

and the C-lobe each of them binding an iron ion hereafter refererred to iron. The lobes alter between open and closed conformation by binding and releasing iron. TrF has been crystallized in three different conformations: open (Noinaj et al., 2012), partially open (Yang et al., 2012), and closed (Wally et al., 2006) (see Fig. 1). It has an open conformation when both lobes are free of iron. In the partially open conformation, in the presence of the transferrin receptor iron is believed to be bound to the N-lobe (Byrne et al., 2010) (Fe_N-TrF) with the C-lobe open. However, in the absence of the transferrin receptor, iron release is faster in N-lobe (Byrne et al., 2010). Therefore, the crystal structure for the partially open conformation has the N-lobe open (Yang et al., 2012) with iron bound to the C-lobe(Fe_C-TrF). Finally, TrF has a closed conformation when iron is bound to both lobes.

Iron release and conformational changes have been studied using a variety of techniques, including small angle scattering (SAS). Before TrF's crystal structures became available, SAS studies indicated that TrF has spheroidal shape (Martel et al., 1980). In the presence and absence of iron, TrF showed differences in SAS curves and distance distribution functions which pointed towards conformational differences (Castellano et al., 1993). Reported values for the radius of gyration were lower in the presence of iron, which suggested a more compact conformation (Grossmann et al., 1992; Kilár and Simon, 1985; Mecklenburg et al., 1997). It has also been reported that the release of iron is pH-dependent and is induced by decreasing pH (Mecklenburg et al., 1997). Moreover, kinetic studies have shown that iron release is influenced by sodium chloride (NaCl). At neutral pH, chloride ions retards iron release, while at acidic pH, it accelerates iron release (HE et al., 2000). In addition, it has been shown that the mechanism of iron release is a complex process that involves cooperativity between the lobes (Abdizadeh et al., 2017; Eckenroth et al., 2011; Mason et al., 2005).

This study is focused on thermal and chemical denaturation of recombinant human transferrin (rTrF) in different pH and salt concentrations and with different co-solutes. These studies are combined with structural analyses performed by small angle X-ray scattering (SAXS) and molecular dynamic (MD) simulations. The SAXS results confirmed previously reported results on the effect of pH and NaCl on the conformation: rTrF shifts towards an open conformation with decreasing pH (Mecklenburg et al., 1997) and with addition of NaCl at low pH (HE et al., 2000), which has a negative impact on overall stability. Moreover, it was shown that arginine, which is used as common stabilizer in protein formulation, binds to rTrF destabilizing the protein as indicated by an up to 20 °C decrease in the temperature of unfolding ($T_{½}$). MD simulations are in agreement with the SAXS results and show that NaCl and arginine induce opening of the N-lobe.

2. Material and methods

2.1. Dialysis and formulation

Recombinant human transferrin (rTrF) was provided by Albumedix Ltd. in 20 g/L solution and was dialyzed into 10 mM histidine pH 5.5, 7.0, and 10 mM tris pH 8.5 for pH and NaCl screening. Concentration of rTrF was measured on a Nanodrop™ 1000 (Thermo Fisher Scientific, Waltham, USA) using extinction coefficient calculated from the primary sequence (Tools et al., 2010) (see Table A.1 in appendix). The dialysed protein was diluted into the final buffer according to the principle shown in Fig. 2: covering pH ± 0.5 in the presence of 0, 70, and 140 mM NaCl. For stability studies with different buffers and excipients, the dialysis was performed at 10 mM histidine pH 5.0 and 6.5, 10 mM acetate pH 5.0, and 10 mM phosphate pH 6.5. Final solutions were obtained by diluting dialysed rTrF into the right buffer: without excipients, with 280 mM sucrose, 140 mM arginine, and 280 mM proline (see Fig. 2).

2.2. Thermal stability studies

Thermal denaturation studies were performed with nano scale differential scanning fluorirmetry (nanoDSF) (Prometheus NT.48, NanoTemper Technologies, Munich, Germany). NanoDSF Grade Standard Capillaries were manually loaded with 10 µl of protein at 1 g/L in the final conditions. All experiments were performed from 20 to 95 °C with a linear thermal ramp using the heating rate of 1 °C/min. Protein intrinsic fluorescence was measured and the unfolding process was monitored by looking at the shift in the fluorescence spectra (350/330 nm). All measurements were done in triplicates and the data analysis was performed using PR.Control v1.12.2 software (NanoTemper Technologies, Munich, Germany).

2.3. Isothermal chemical denaturation

All chemical denaturation studies were performed using automated fluorescence-based protein denaturation system (HUNK - AVIA ICD 2304, Unchained Labs, Pleasanton, USA). The excitation wavelength was 285 nm, and emission intensities were recorded from 300 nm to 450 nm. The gain setting was set for 100, based on a previously

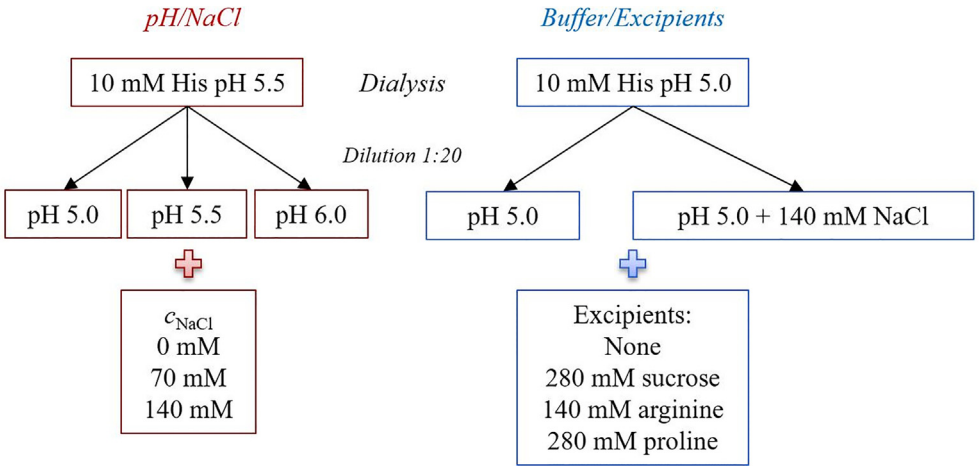

Fig. 2. Schematic representation of the principle for dialysis and formulation process. (For interpretation of the references to colour in this figure legend, the reader is referred to the web version of this article.)

performed gain test. From the incubation test, 162 min of additional incubation time was used. 48-point linear gradient of denaturant was automatically generated for each condition. For the pH and NaCl screening urea and guanidine hydrochloride (GuHCl) were used as denaturants, while for the buffer and excipient screening GuHCl was selected. 10 M urea and 6 M GuHCl stock solutions were prepared in each tested condition. Protein stock solutions were prepared at 1 g/L and were subsequently diluted 12.5 times to the final condition. Data collection and analysis were performed using Formulator software v3.02 (Unchained Labs, Pleasanton, USA). Protein intrinsic fluorescence was measured and the unfolding process was monitored by looking at the shift in the fluorescence spectra (356/318 nm) with increasing GuHCl concentration. Despite poorly defined intermediate states, 3-state models showed better fit and lower errors than 2-state models, and therefore 3-state models were selected for data analysis. In order to minimize the error, a secondary fit was performed for each pH value combining different NaCl concentrations. Free energy of unfolding (ΔG_{unfold}), $c_{½}$, and *m*-values were calculated for both transitions.

2.4. Microscale Thermophoresis

MicroScale Thermophoresis (MST) was performed using Monolith NT.115 Label Free system through the MO.Control software (NanoTemper Technologies, Germany). All measurements were carried out in 10 mM acetate pH 5.0 at 25 °C and two different ligands were chosen: arginine and proline with stock concentration of 1 M each. Each standard capillary was manually loaded with 10 µl of protein at 1 µM with different ligand concentrations, covering the concentration range from 500 to 0.78 mM. All measurement were carried out at 20% excitation power. Data analysis was done using the software MO. Affinity analysis. Initial fluorescence was used for data evaluation. For the arginine binding curve and K_d calculation eight independent experiments were performed. Proline binding affinity experiments were performed in triplicates.

2.5. Size exclusion chromatography coupled to multi-angle light scattering (SEC-MALS)

A Vanquish Horizon™ UPLC system with a variable wavelength UV detector was operated at 280 nm (Thermo Fischer Scientific, Waltham, USA). All experiments were performed at 4 °C and temperature was controlled by autosampler. The separation was performed with a Superdex 200 increased 10/30 GL column. The aqueous mobile phase consisted of 38 mM NaH_2PO_4, 12 mM Na_2HPO_4, 150 mM NaCl and 200 ppm NaN_3 at pH 7.4 dissolved in HPLC-grade water. The mobile phase was filtered through Durapore VVPP 0.1 µm membrane filters (Millipore Corporation, Billerica, MA, USA). All the samples were centrifuged and injected in duplicates at a volume of 25 µl. Immediately after exiting the column, samples passed through the UV detector followed by static light scattering apparatus, a TREOS MALS detector (Wyatt Technology, Santa Barbara, USA), and differential refractive index detector (Optilab T-rEX, Wyatt Technology, Santa Barbara, USA). Data collection and processing were performed using the ASTRA® software V7.2 (Wyatt Technology, Santa Barbara, USA.

2.6. Small angle X-ray scattering

Data collection was performed at the P12 beamline at the Petra III storage ring (DESY, Hamburg DE) (Blanchet et al., 2015) and at the BM29 beamline (ESRF, Grenoble FR) (Round et al., 2008) (see Table A.1 in appendix). Radius of gyration (R_g) and maximum dimension (D_{max}) were derived from the experimental data with the graphical data analysis program *PRIMUSQT* (Petoukhov et al., 2012).

The rTrF crystal structures are available in three conformations in the protein data bank (Berman et al., 2006), *i.e*, partially open (PDB ID: 3QYT (Yang et al., 2012)), closed (PDB ID: 3V83 (Noinaj et al., 2012)), and open (PDB ID: 2HAU (Wally et al., 2006)) conformations.

Rigid body modelling of the dimer was performed using *SASREFMX* (Petoukhov et al., 2012) (see Fig. A.7 in appendix), using the crystal structure of the closed conformation (3V83) as dissociation product. The data was fit against two merged curves: from histidine pH 6.5 and tris pH 8.0, where only closed conformation of the monomer was observed (see Fig. A.8 in appendix). In order to calculate the volume fractions of each component in the mixture, the data program *OLIGOMER* (Petoukhov et al., 2012) was used. *FFMAKER* (Petoukhov et al., 2012) was used to create an input file for *OLIGOMER* with a form factor for each component (open, partially open, and closed comformations retrieved from the protein data bank (Berman et al., 2006) and dimer from *SASREFMX* as input).

2.7. Molecular dynamics simulation

The closed rTrF crystal structure was obtained from the protein data bank (Berman et al., 2006) (PDB ID: 3V83 (Noinaj et al., 2012)). This conformation was used as a start structure for molecular dynamics (MD) simulations. The Fe^{3+} ion and bicarbonate (CO_3^{2-}) molecules were included in the simulations. The structure was initially prepared at pH 5.0 and pH 6.5 using the H++ server (http://biophysics.cs.vt.edu/H++) (Gordon et al., 2005) which accounts for the protonation state

of the titratable residues. Full details of the setup of the MD simlations has been described previously (Indrakumar et al., 2019). The excipients acetate, phosphate, arginine, histidine, sodium chloride were included in the study. Structures were obtained from PubChem (Kim et al., 2019) and Zinc Database (Irwin et al., 2012). These molecules were prepared at the desired pH using ligprep tool in Schrödinger 2016-3 suite (Schrödinger, LLC, New York, NY, USA) (Madhavi Sastry et al., 2013). Parameter file for the excipients and bicarbonate wereprepared using the antechamber (Wang et al., 2004) module in Amber 16 at desired pH. Charges were estimated using the AM1-BCC (Jakalian et al., 2002) charge method. Using the 12-6-4 LJ-type nonbonded (Li and Merz, 2014; Panteva et al., 2015) model in the amber force field, parameters for Fe^{3+} were obtained. All-atom classical constant pH molecular dynamics simulations (Mongan et al., 2004) in explicit solvent were carried out with the Amber 16 program (Maingi et al., 2012) employing the amber force field ff99SB (Lindorff-Larsen et al., 2010) for proteins. Titratable residues such as Asp, His, Lys, Tyr, surrounding the Fe^{3+} and the bicarbonate were titrated during the simulations. Ionic strength for each of the excipients was adjusted to 140 mM by additions of 124 solute molecules to the solvated system containing approximately 48,000 water molecules. Finally, constant pH simulations were performed for 100 ns and coordinates were saved every 10 ps. Analyses were performed with CPPTRAJ (Roe and Cheatham, 2013) in Amber 16, and VMD version 1.9.3 (Humphrey et al., 1996).

Preferential interaction coefficient (PIC) for the specific simulated system was calculated using the method described previously (Indrakumar et al., 2019). Furthermore, an interaction score per $P(I_{score})$ was calculated to estimate binding capacity of co-solute to residues on protein surface as described. Center of mass of the co-solute was used for the determination of PIC and $P(I_{score})$.

3. Results

The overall conformational stability of recombinant transferrin (rTrF) was analyzed by thermal denaturation using nano differential scanning fluorimetry (nanoDSF) and isothermal chemical denaturation (ICD). Two different denaturants, urea and guanidine hydrochloride (GuHCl) were tested. Due to the high conformational stability of rTrF, urea was not strong enough to unfold it completely (see Fig. 3C). Therefore, only GuHCl unfolding data were analyzed. The initial screen was performed as a function of pH (5–9) and ionic strength (0, 70, and 140 mM NaCl). NanoDSF thermal unfolding shows a single two-step transition (from folded to unfolded state), while chemical denaturation curves demonstrate the presence of an intermediate state, resulting in a three-state transition. In addition, the intermediate state is better defined at lower pH values (see Fig. 3B). Only the first transition in the chemical unfolding curves was further considered, as this is where unfolding process is initiated. Due to the poorly defined intermediate state, the calculated ΔG_{unfold} shows high standard deviations and was therefore not considered for analysis.

3.1. pH dependence

$T_{½}$ measured by nanoDSF is shown in Fig. 4A. An increase in $T_{½}$ with increasing pH is seen, meaning that the thermal stability is higher at higher pH values. Likewise, chemical denaturation shows an increase in the amount of GuHCl needed to unfold 50% of the protein ($c_{½}$) with increasing pH values (see Fig. 4B).

In order to study conformational changes, SAXS concentration series data were collected at pH 4.0, 5.0, 6.5 and 8.0 with 0 mM NaCl (see Table A.2 in appendix). All scattering curves and SAXS data analyses are shown in the appendix (see Fig. A.1). At pH 6.5 and 8.0, the curves coincide and the intensity at low q-values decreases with increasing rTrF concentration, indicating a repulsive system. Contrary to this, at pH 5.0 in histidine the intensity shows a small increase with rTrF concentration, which is characteristic for the presence of small amounts of aggregates. Both aggregation and repulsion are observed at pH 4.0 (see Fig. A.1A in appendix).

Moreover, four representative curves (shown in Fig. 5) differ in shape depending on pH, which indicates conformational dissimilarity. Finally, we observe that the estimated molecular weight (*MW*) at 1 g/L for most of the conditions is higher than the expected: 75 kDa (see Table A.3 in appendix), which means that a substantial fraction of the protein molecules form larger species.

In order to characterize the size of the larger species, SEC-MALS was performed (see Table A.4 and Fig. A.2 in appendix), confirming the presence of approximately 12%, dimer and 2% trimer at all tested conditions. Additionally, static light scattering was performed as a function of protein concentration showing a concentration independent *MW* (see Fig. A.9 in appendix).

It is known that rTrF exists in different conformations: open, partially open, and closed, which is related to iron binding and release (Kilár and Simon, 1985). In order to evaluate the rTrF conformation at different pH values, *OLIGOMER* (Konarev et al., 2003) analysis was performed using pdbid: 2HAU (Wally et al., 2006) for the closed conformation, pdbid: 3QYT (Yang et al., 2012) for the partially open conformation (Fe_C-rTrF) and pdbid: 3V83 (Noinaj et al., 2012) for the completely open conformation as input, while the dimer was modelled by *SASREFMX* (Petoukhov et al., 2012). Due to the very small amounts of trimer, this species was not taken into consideration.

The analysis is seen in Fig. 6 (see also Table A.5 in appendix), showing that at 10 mM histidine pH 6.5 and 10 mM tris pH 8.0 rTrF is in the closed conformation (Fig. 6D and E). At 10 mM acetate pH 5.0 and 10 mM histidine pH 5.0 rTrF is present in closed and partially open conformation (Fig. 6B and C).

By changing to 10 mM acetate buffer pH 4.0, it allowed us to detect

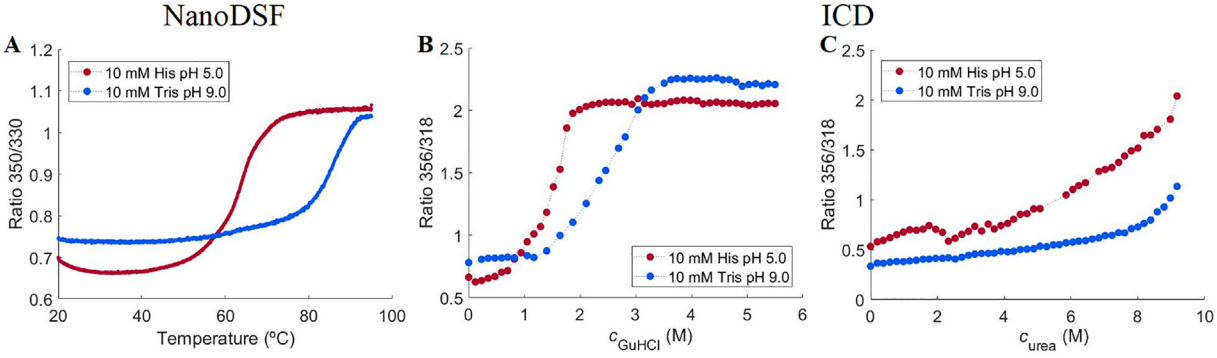

Fig. 3. rTrF thermal and chemical unfolding curves. A: thermal unfolding curves from nanoDSF, B: chemical unfolding curves in the presence of GuHCl from ICD and C: chemical unfolding curves in the presence of urea from ICD. rTrF in 10 mM histidine (His) pH 5.0 (red), and 10 mM tris pH 9.0 (blue). (For interpretation of the references to colour in this figure legend, the reader is referred to the web version of this article.)

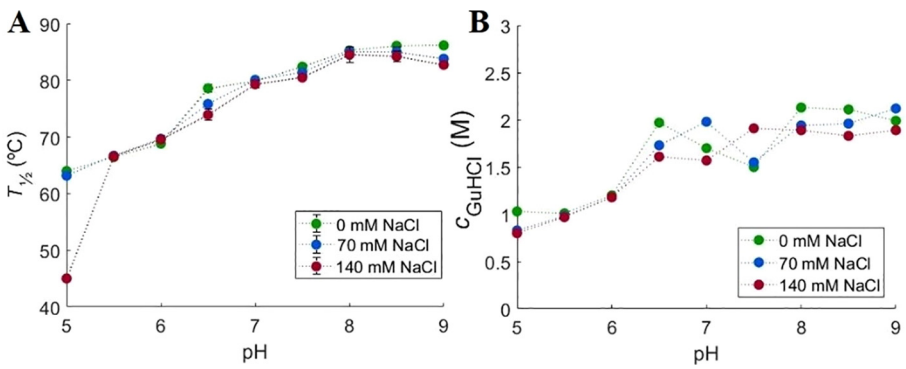

Fig. 4. Initial stability studies performed by NanoDSF and ICD at different pH and ionic strengths. A: changes in $T_{½}$ and B: changes in $c_{½}$ with pH in the presence of 0 mM (green), 70 mM (blue), and 140 mM (red) NaCl. (For interpretation of the references to colour in this figure legend, the reader is referred to the web version of this article.)

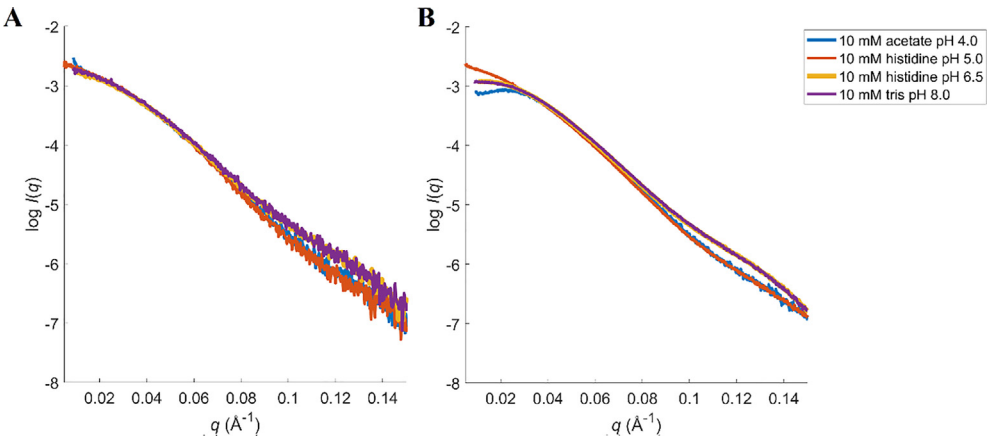

Fig. 5. Comparison of SAXS curves from A: $c_{rTrF} \sim 1$ g/L and B: $c_{rTrF} \sim 10$ g/L collected at different pH. Blue: 10 mM acetate pH 4.0; orange: 10 mM histidine pH 5.0; yellow: 10 mM histidine pH 6.5; and purple: 10 mM tris pH 8.0. (For interpretation of the references to colour in this figure legend, the reader is referred to the web version of this article.)

a small amount of the open conformation (see Fig. 6A). In order to reduce the effect of repulsion/aggregation in *OLIGOMER* analysis, the first points, where the effect of aggregation/repulsion is seen, were removed.

3.2. NaCl dependence

Overall thermal stability is independent of the NaCl concentration, except at pH 5.0, where 140 mM NaCl cause a decrease in $T_{½}$ from 65 °C to 45 °C (see Fig. 4A). At higher pH values the addition of NaCl does not show any effect. The ICD experiments did not show an NaCl effect on $c_{½}$.

SAXS experiments were performed at 5 g/L rTrF in 10 mM histidine pH 5.0 and 6.5 with increasing NaCl concentrations (see Fig. 6F and G). At pH 5.0, a gain in $I(0)$ is seen with increasing c_{NaCl} due to rising *MW* (up to 100 kDa), which points to the presence of aggregates (see Table A.3 in appendix). The *OLIGOMER* shows an increase in the volume fraction of higher *MW* species (see Fig. 6F). The observation of larger aggregates is in agreement with NanoDSF and ICD results showing lower conformational stability at pH 5.0 with increasing salt concentration. At pH 6.5, the repulsion decreases when NaCl is added, leading to higher $I(0)$ (see Fig. A.1H in appendix).

3.3. Buffer and excipient dependence

For the investigations of excipient and buffer effects histidine buffer at pH 5.0 and 6.5 with 0 or 140 mM NaCl, as well as acetate pH 5.0 and phosphate pH 6.5 were selected. Furthermore, three different excipients: 280 mM sucrose, 140 mM arginine, and 280 mM proline were tested.

$T_{½}$ from nanoDSF and $c_{½}$ from ICD are shown in Fig. 7. With respect to the buffer dependence effect, it is seen that at pH 5.0 rTrF has a 5 °C higher $T_{½}$ in acetate buffer compared to histidine buffer, while addition of 140 mM NaCl to the histidine buffer decreases $T_{½}$ by 15 °C. The ICD measurements show a somewhat different picture for histidine buffer as the addition of NaCl does not influence $c_{½}$, which is already significantly lower in the histidine buffer compared to the acetate buffer.

At pH 6.5, $T_{½}$ is about 15 °C higher in histidine buffer than in phosphate buffer. Addition of 140 mM NaCl to the histidine buffer decreases $T_{½}$ by 5 °C. The ICD results are similar as $c_{½}$ is reduced by 1 M in phosphate buffer, while in histidine buffer, addition of NaCl only leads to a very small decrease.

Adding sucrose or proline at pH 5.0 leads to minor effects on $T_{½}$. In contrast, arginine has enormous impact on rTrF stability. Addition of arginine leads to a decrease of $T_{½}$ by 20–25 °C at pH 5.0 except when 140 mM NaCl is present. Both arginine and 140 mM NaCl reduce $T_{½}$ by around 20 °C, however, adding both of them together does not alter this already low $T_{½}$ (see Fig. 7A). Chemical denaturation shows a different picture, where addition of excipients in histidine buffer does not have an effect on $c_{½}$. In acetate buffer $c_{½}$ is 1.6 M and addition of arginine or proline leads to a decrease of $c_{½}$ by approximately 1 M.

At pH 6.5 arginine decreases $T_{½}$ by 5–10 °C in histidine buffer, but has no effect in phosphate buffer, where $T_{½}$ is already low. Excipients do not show an effect on $c_{½}$ at pH 6.5 in both buffers (see Fig. 7D).

The negative effect of arginine on the thermal rTrF stability can be explained by arginine binding to the protein. This was tested by performing MST using proline as a negative control, which does not have a significant effect on thermal stability. MST results show that arginine binds weakly to rTrF with K_d of 0.180 M (see Fig. 8).

SAXS data were collected for rTrF in acetate and histidine buffers at pH 5.0 (see Fig. A.1 in appendix) and analyzed using *OLIGOMER* (see Fig. 6C and B, and Table A.5 in appendix). In both buffers, partially open and closed conformations are present, with the volume fraction of the partially open conformation decreasing with increasing rTrF concentration. However, acetate buffer shows higher volume fractions of closed conformation.

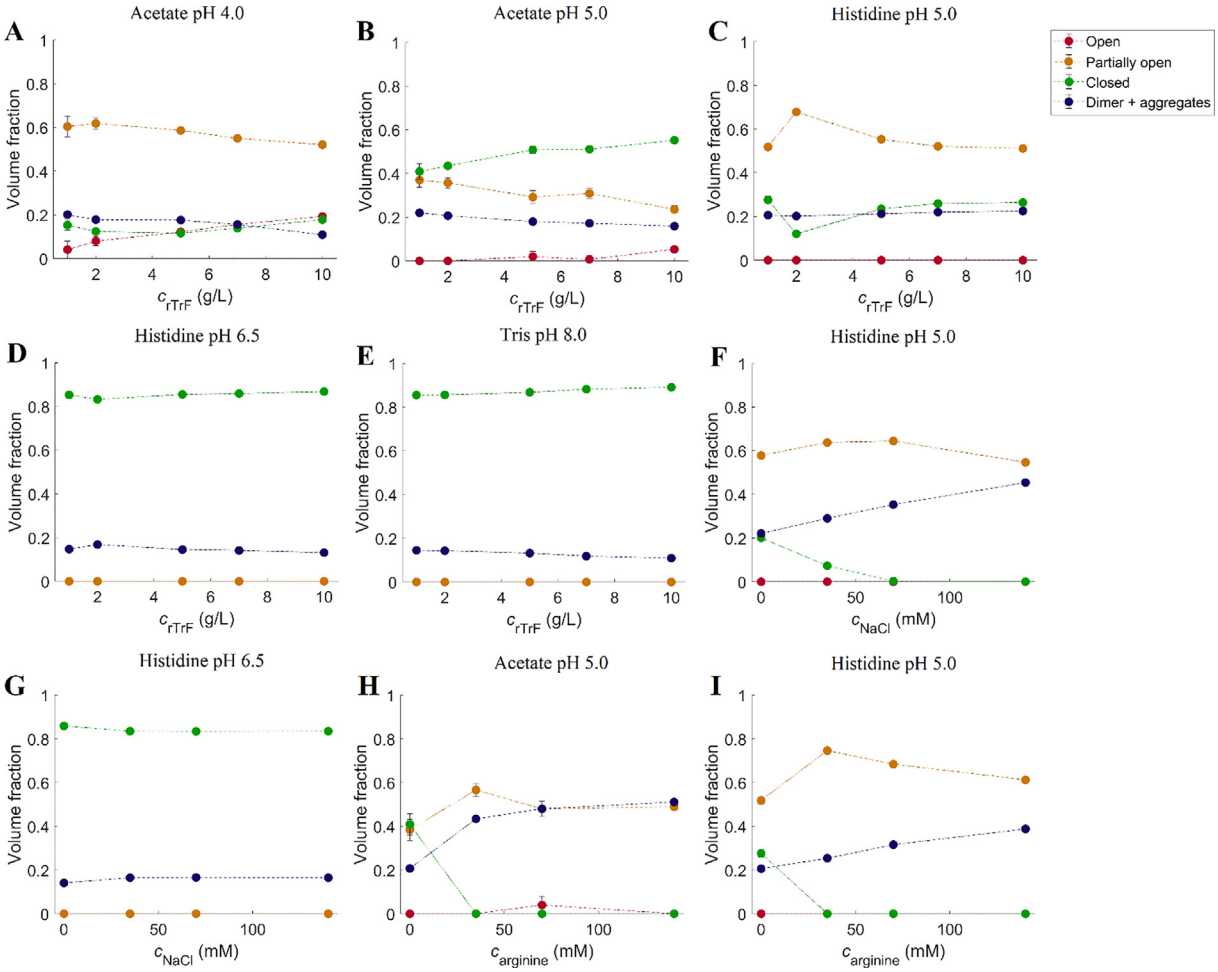

Fig. 6. Fraction of different monomer conformations (open (in red), partially open (in orange), and closed (in green)) and dimer (in blue). A: acetate pH 4.0; B: acetate pH 5.0; C: histidine pH 5.0; D: histidine pH 6.5; E: tris pH 8.0; F: 5 g/L rTrF, histidine pH 5.0 with NaCl; G: 5 g/L rTrF, histidine 6.5 with NaCl; H: 5 g/L rTrF, acetate 5.0 with arginine; I: 5 g/L rTrF, histidine 5.0 with arginine. (For interpretation of the references to colour in this figure legend, the reader is referred to the web version of this article.)

3.4. Molecular dynamics simulations

In order to understand the interactions between rTrF and the other components in the solution at selected pH and buffer conditions, MD simulations were performed in the presence of NaCl, histidine, arginine, acetate, and phosphate.

MD simulations were performed for 100 ns in the presence of bound Fe^{3+} and carbonate (CO_3^{2-}) in both lobes. All systems reached a constant root mean square deviation after 3 ns (data not shown). Patches that comprise at least three residues structurally close on the protein surface and have moderately strong interactions are colored based on $P(I_{score})$ (see Fig. 9). $P(I_{score})$ given to a residue helps to deduct the preference of different additives on the protein surface, which in turn leads to an understanding of the different mechanism related to stabilization and iron release. At pH 5.0, both arginine and histidine are positively charged (+1), while acetate is negatively charged (-1). Even though excipients interact with the protein at several regions, only few patches interacting with the additives are relatively large and strong. Generally, arginine, histidine, and NaCl have stronger interactions in the C-lobe as compared to acetate, which interacts stronger in the N-lobe. A particular region on the C-lobe that is a common interaction site for the different buffer components consists of residue D416 and D420 (see Fig. 9A, B, and C).

At pH 6.5, phosphate, when compared to histidine, shows stronger interacting patches on the protein surface that are highlighted in the Fig. 9E.

4. Discussion

4.1. pH effect

pH-dependent conformational changes in rTrF are aligned with its physiological function that is binding and transporting iron into the cells. Due to the high toxicity of iron, it is important that rTrF remains in the closed conformation in blood (de Jong et al., 1990). Blood has a pH of 7.4 where according to the SAXS data only the closed conformation is present. However, rTrF should be able to supply cells with iron. Iron release occurs under acidic condition in the endosome (Bali et al., 1991; Sipe and Murphy, 1991), where the pH is around 5 (Hu et al., 2015). SAXS data analysis shows presence of the partially open conformation at pH 5.0, which supports conclusions of previous studies that prove conformational changes of rTrF being pH-dependent (Mecklenburg et al., 1997). Our SAXS studies do not show evidence of the presence of a fully open conformation at pH 5.0. At pH 4.0, a small fraction of fully open conformation was detected, accompanied by increasing aggregation (see Fig. A.1A in appendix). This suggests that the presence of the fully open conformation may induce aggregation and therefore, it is important to have a mechanism that reduces the possibility of full opening of rTrF. This data supports that iron release is not only pH-dependent but also involves cooperativity between the N- and

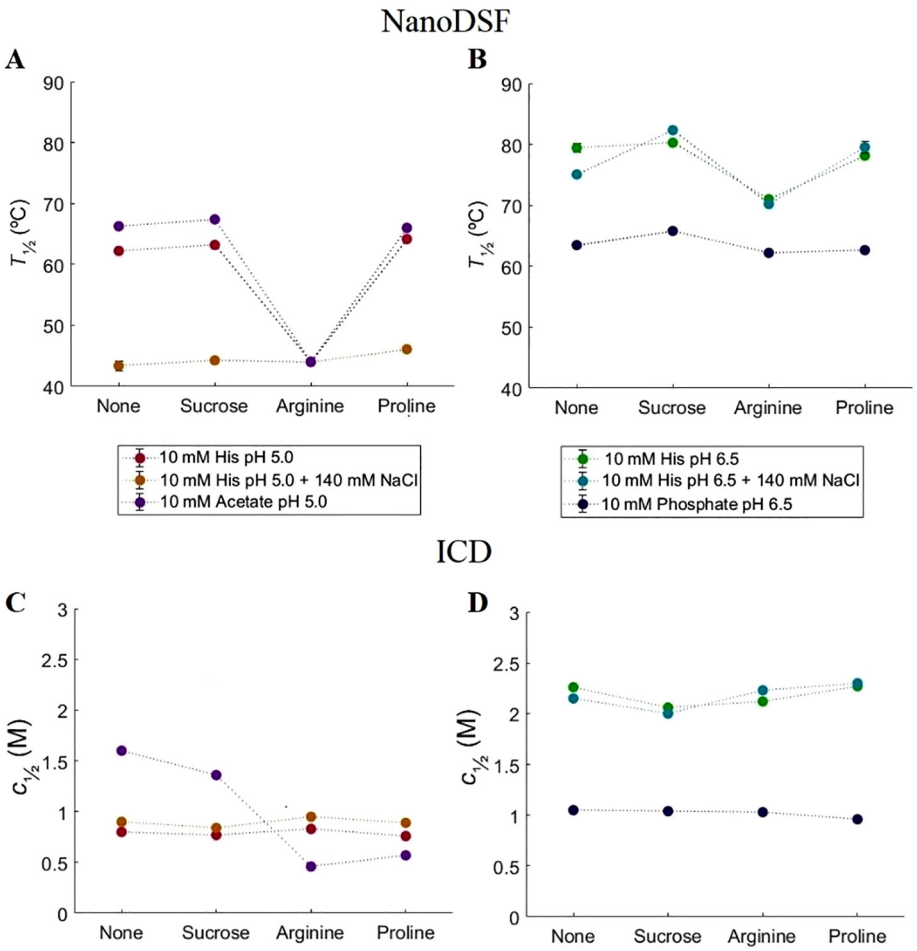

Fig. 7. NanoDSF and ICD stability studies using different buffers and excipients. Purple: 10 mM acetate pH 5.0; red 10 mM histidine pH 5.0; orange: 10 mM histidine pH 5.0 with 140 mM NaCl; blue: 10 mM phosphate pH 6.5; green: 10 mM histidine pH 6.5; cyan: 10 mM histidine pH 6.5 with 140 mM NaCl. A: changes in $T_{½}$ at histidine (0 and 140 mM NaCl) and acetate pH 5.0; B: changes in $T_{½}$ at histidine (0 and 140 mM NaCl) and phosphate pH 6.5; C: changes in $c_{½}$ at histidine (0 and 140 mM NaCl) and acetate pH 5.0; D: changes in $c_{½}$ at histidine (0 and 140 mM NaCl) and phosphate pH 6.5. (For interpretation of the references to colour in this figure legend, the reader is referred to the web version of this article.)

the C-lobe (Abdizadeh et al., 2017; Eckenroth et al., 2011; Mason et al., 2005).

Thermal and chemical denaturation showed a decrease in physical stability with decreasing pH, at which the partially open conformation is present. Since this conformation has a higher solvent-accessible surface area than the closed conformation, it may unfold more easily.

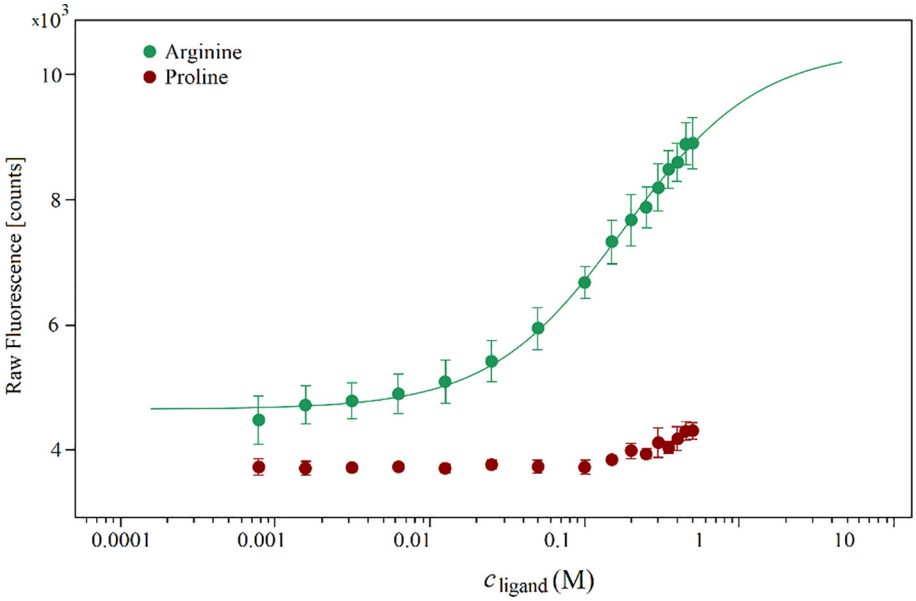

Fig. 8. MST binding curve for arginine (in green) from K_d-fit using proline (in red) as a negative control. (For interpretation of the references to colour in this figure legend, the reader is referred to the web version of this article.)

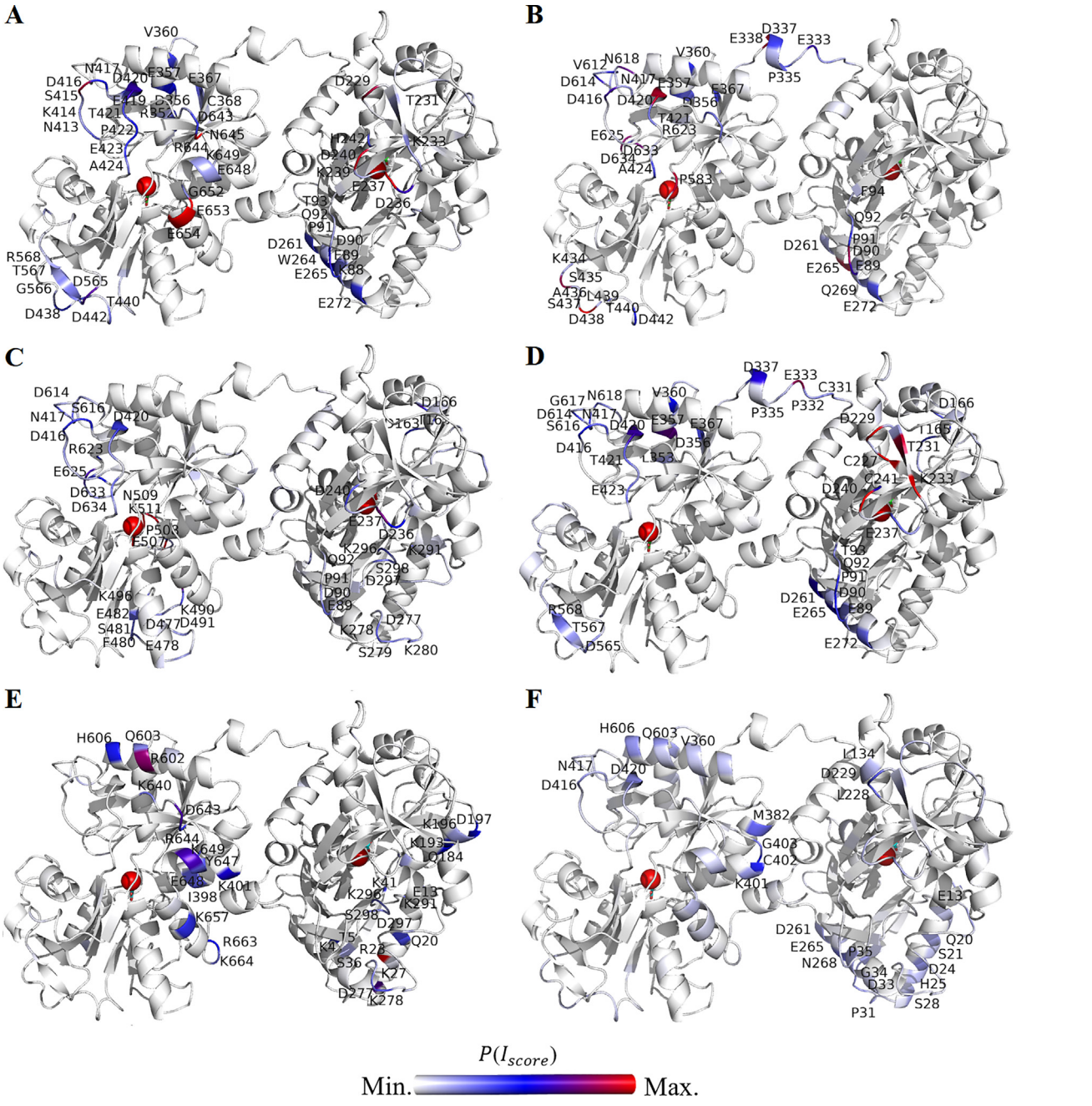

Fig. 9. The closed structure of rTrF colored at the patches interacting strongly with buffer components based on the $P(I_{score})$ calculated at pH 5.0. A: arginine, B: histidine, C: NaCl, and D: acetate; and at pH 6.5 for E: phosphate, and F: histidine. The C-lobe is shown on the left and the N-lobe on the right. Single letter code for aminoacids is used. (For interpretation of the references to colour in this figure legend, the reader is referred to the web version of this article.)

4.2. NaCl effect

With addition of NaCl, $T_{½}$ at pH 5.0 decreases by 20 °C and SAXS data indicate aggregation of rTrF. As already noted, at pH 5.0 both partially open and closed conformation are present. Addition of NaCl decreases the volume fraction of the closed conformation, and increases the one of the partially open conformation with the N-lobe open (see Fig. 6F).

Opening of the N-lobe can be explained by interactions of NaCl at the entrance of the N-lobe cleft. Especially, the loop regions (residues 89–94, 236–240, 277–280, and 296–298), are prone to interact with salt ions. Previous studies have shown that crosstalk between the lobes leads to iron release first occurring from the N-lobe (Byrne et al., 2010; Eckenroth et al., 2011). At this end, interaction in the C-lobe loop region (D416, D420) might be inducing conformational changes that affect iron release from the N-lobe (see Fig. 9C).

This is in agreement with previous studies, where NaCl has been proven to accelerate iron release at acidic pH, due to the higher anion-binding affinity of rTrF (HE et al., 2000) when compared to higher pH. In addition, presence of the partially open conformation, which has lower stability, contributes to the aggregation process.

At higher pH values the presence of NaCl does not induce significant changes in thermal stability. The SAXS studies confirmed that rTrF is only present in the compact conformation at pH 6.5, and that the addition of NaCl has no impact (see Fig. 6G). In a previous study, chloride was shown to slow down iron release at neutral pH (HE et al., 2000).

4.3. Excipient effect

Amongst the tested excipients, arginine has a pronounced negative effect on the stability of rTrF, especially at pH 5.0 where $T_{½}$ decreases by 20 °C and $c_{½}$ is reduced by 1 M. According to SAXS results, the the fraction of partially open conformation increases at the expense of the closed conformation (see Fig. 6H and I, and Table A.5 in appendix), leading to an aggregation. MST confirms arginine binding to rTrF at pH 5.0. MD simulations show that arginine interacts with the protein in several regions (see Fig. 9A). Adding proline in acetate has a slightly destabilizing effect seen in ICD $c_{½}$, but not in $T_{½}$. Furthermore, MST did not show binding of proline.

4.4. Buffer effect

The buffer type has a clear effect on the protein stability (Wang, 1999). At pH 5.0, replacing histidine by acetate buffer positively affects rTrF stability, while at pH 6.5, histidine buffer is preferable over phosphate buffer.

SAXS studies show that acetate buffer at pH 5.0 stabilizes the closed conformation compared to histidine buffer and the volume fractions increases from 0.3 to 0.4 (see Fig. 6B and C, and Table A.5 in appendix). The reason for this change in equilibrium is difficult to explain from the MD studies, but acetate shows stronger interactions with the N-lobe around 227–241 compared to the histidine, and less interactions in the C-lobe. Additionally, in the presence of histidine, rTrF shows higher flexibility in N-lobe (see Fig. A.10 in appendix).

As already mentioned, at pH 5.0, arginine and NaCl shift the equilibrium from the closed to the partially open conformation. All of them interact with regions in the N-lobe, particularly around the iron binding cleft comprising of loop region (89–94 and 236–240, see Table 1), which might lead to conformational changes and induce its opening, resulting in the lower stability. Additionally, they have one common interaction patch comprising D416 and D420 and others residues around (Fig. 9A and C, and Table 1), pointing to a crucial role in rTrF's conformational changes. These residues are present on the loop region close to C-lobe cleft, but not directly connecting the two subdomains. However, this loop is prone to high fluctuations as reflected in MD simulations (data not shown) and might be involved in the cooperativity between two lobes, since conformational changes in this region can lead to lobe-lobe interaction, and contribute to the N-lobe opening.

At pH 6.5 both phosphate and histidine have weak to negligible interactions in the loop region of the C-lobe and also in the loop region (89–94) of the N-lobe (see Fig. 9E and F). In both buffers, rTrF is present only in the closed conformation, pointing to the involvement of these two loops (89–94 and 416–420) in the iron release mechanism. Phosphate has a destabilizing effect compared to histidine, which might be due to few patches interacting strongly with phosphate on the protein surface. The preferential interaction coefficient values are higher for phosphate as compared to histidine implying higher preference of the protein surface for phosphate (see Fig. A.3 in appendix).

5. Conclusion

The presented work is a systematic study of the overall physical behavior of rTrF in a variety of different buffer conditions combined with structural studies using SAXS and MD simulations. The increase of $T_{½}$ and $c_{½}$ are both indicators of increased conformational stability. Although, some of the trends seem to be similar for these two indicators, some specific differences are seen probably because in one experiment temperature increases and in the other experiment a chemical compound is added (GuHCl). However, combining denaturation results with volume fractions of closed and partially open conformations seen in the SAXS studies (see Fig. 10), it is possible to observe a decrease in volume fraction of the partially open conformation with increasing $T_{½}$ and $c_{½}$, and a corresponding increase in volume fraction of the closed conformation. Several conditions, such as the presence of arginine, NaCl, buffers, and pH changes can lead to opening and, consequently, to a decrease in rTrF stability. MD simulations indicate that this occurs due to the binding of the additives to regions in the N-lobe cleft, as well as a loop in the C-lobe, causing the N-lobe to open.

Author contributions

Alina Kulakova collected all SAXS, nanoDSF, MST, and ICD data and performed formal analysis on these. She wrote original draft and edited the manuscript. Sowmya Indrakumar performed molecular dynamic simulations and wrote that part of the manuscript. Pernille Sønderby contributed with data interpretation for small angle X-ray scattering. Lorenzo Gentiluomo collected SEC-MALS data and performed formal analysis of these. Günther Peters supervised MD simulation studies and participated in SAXS data collection. Pernille Harris contributed with funding acquisition, conceptualization, and supervision. Commented and edited the manuscript. Dierk Roessner supervised LG and the light scattering experiments. Wolfgang Friess supervised LG. Werner Streicher supervised stability studies. All the authors contributed with review and comments on the manuscript.

Declaration of Competing Interest

The authors declare that they have no known competing financial interests or personal relationships that could have appeared to influence the work reported in this paper.

Acknowledgements

EMBL P12 DESY and EMBL B29 ESRF for providing beam time for performing the SAXS experiments.

Albumedix Ltd for kindly providing us with recombinant transferrin.

This work was supported by European Union's Horizon 2020 research and innovation program (grant agreement nr 675074) and DanScatt.

Simulations were performed at the high performance computing (HPC) services at DTU and in-house CPU/GPU cluster facilities at DTU

Table 1
Summary of the stability studies from nanoDSF ($T_{½}$) and ICD ($c_{½}$) and structural studies from MD (main interacting patches) and SAXS (volume fractions).

	Stability studies		Structural studies				
			MD (interacting patches)		SAXS (volume fractions)		
	$T_{½}$ (°C)	$c_{½}$ (M)	N-lobe	C-lobe	Partially open	Closed	Dimer + aggregates
Histidine	62.2	1.2	E89-F94	D416-D420	0.5	0.3	0.2
NaCl	43.4	1.14	E89-F94, D236- D240, D277- K280, K291-S298	D416-D420	0.5	0	0.5
Acetate	66.3	1.35	E89-T93, C227-C241	D416-D420	0.4	0.4	0.2
Arginine	44.1	1.74	K88-T93, D229-K233, D236-H242	N413-Q424	0.6	0	0.4

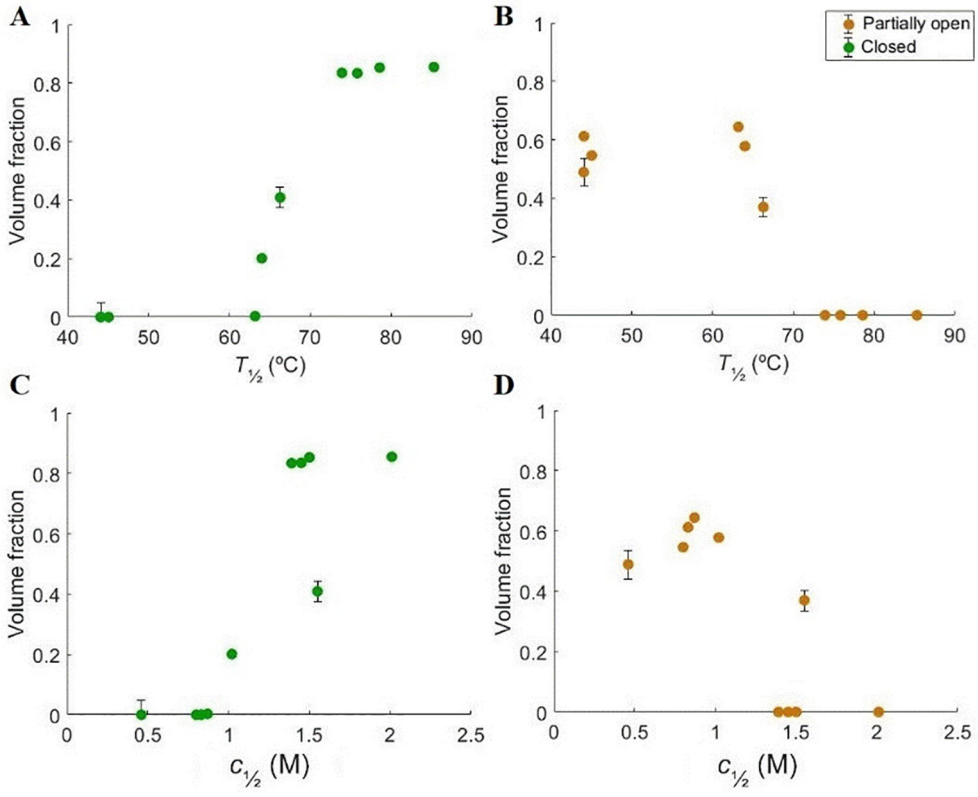

Fig. 10. Volume fractions of different rTrF species correlated to thermal and chemical denaturation studies. A and B: volume fractions correlated to $T_{½}$; C and D: volume fractions correlated to $c_{½}$. Partially open conformation colored in orange and closed conformation colored in green. (For interpretation of the references to colour in this figure legend, the reader is referred to the web version of this article.)

Chemistry.

Appendix A. Supplementary data

Supplementary data to this article can be found online at https://doi.org/10.1016/j.yjsbx.2019.100017.

References

Abdizadeh, H., Atilgan, A.R., Atilgan, C., 2017. Mechanisms by which salt concentration moderates the dynamics of human serum transferrin. J. Phys. Chem. B 121, 4778–4789. https://doi.org/10.1021/acs.jpcb.7b02380.

Bali, P.K., Zak, O., Aisen, P., 1991. A new role for the transferrin receptor in the release of iron from transferrin. Biochemistry 30, 324–328. https://doi.org/10.1021/bi00216a003.

Berman, H.M., Westbrook, J., Feng, Z., Gilliland, G., Bhat, T.N., Weissig, H., Shindyalov, I. N., Bourne, P.E., 2006. The Protein Data Bank, 1999–, in: International Tables for Crystallography. International Union of Crystallography, Chester, England, pp. 675–684. doi: 10.1107/97809553602060000722.

Blanchet, C.E., Spilotros, A., Schwemmer, F., Graewert, M.A., Kikhney, A., Jeffries, C.M., Franke, D., Mark, D., Zengerle, R., Cipriani, F., Fiedler, S., Roessle, M., Svergun, D.I., 2015. Versatile sample environments and automation for biological solution X-ray scattering experiments at the P12 beamline (PETRA III, DESY). J. Appl. Crystallogr. 48, 431–443. https://doi.org/10.1107/S160057671500254X.

Byrne, S.L., Chasteen, N.D., Steere, A.N., Mason, A.B., 2010. The unique kinetics of iron release from transferrin: the role of receptor, lobe-lobe interactions, and salt at endosomal pH. J. Mol. Biol. 396, 130–140. https://doi.org/10.1016/j.jmb.2009.11.023.

Castellano, A.C., Barteri, M., Bianconi, A., Borghi, E., Cassiano, L., Castagnola, M., Della Longa, S., 1993. X-ray small angle scattering of the human transferrin protein aggregates. A fractal study. Biophys. J. 64, 520–524. https://doi.org/10.1016/S0006-3495(93)81394-8.

de Jong, G., van Dijk, J.P., van Eijk, H.G., 1990. The biology of transferrin. Clin. Chim. Acta. doi: 10.1016/0009-8981(90)90278-Z.

Eckenroth, B.E., Steere, A.N., Chasteen, N.D., Everse, S.J., Mason, A.B., 2011. How the binding of human transferrin primes the transferrin receptor potentiating iron release at endosomal pH. Proc. Natl. Acad. Sci. 108, 13089–13094. https://doi.org/10.1073/pnas.1105786108.

Fishman, J.B., Rubin, J.B., Handrahan, J.V., Connor, J.R., Fine, R.E., 1987. Receptor-mediated transcytosis of transferrin across the blood-brain barrier. J. Neurosci. Res. 18, 299–304. https://doi.org/10.1002/jnr.490180206.

Gordon, J.C., Myers, J.B., Folta, T., Shoja, V., Heath, L.S., Onufriev, A., 2005. H++: a server for estimating pKas and adding missing hydrogens to macromolecules. Nucl. Acids Res. 33, W368–W371. https://doi.org/10.1093/nar/gki464.

Grossmann, J.G., Neu, M., Pantos, E., Schwab, F.J., Evans, R.W., Townes-Andrews, E., Lindley, P.F., Appel, H., Thies, W.-G., Hasnain, S.S., 1992. X-ray solution scattering reveals conformational changes upon iron uptake in lactoferrin, serum and ovotransferrins. J. Mol. Biol. 225, 811–819. https://doi.org/10.1016/0022-2836(92)90402-6.

He, Q.-Y., Mason, A.B., Nguyen, V., Macgillivray, R.T.A., Woodworth, R.C., 2000. The chloride effect is related to anion binding in determining the rate of iron release from the human transferrin N-lobe. Biochem. J. 350, 909–915. doi: 10.1042/bj3500909.

Hu, Y.B., Dammer, E.B., Ren, R.J., Wang, G., 2015. The endosomal-lysosomal system: From acidification and cargo sorting to neurodegeneration. Transl. Neurodegener., doi: 10.1186/s40035-015-0041-1.

Humphrey, W., Dalke, A., Schulten, K., 1996. VMD: Visual molecular dynamics. J. Mol. Graph. 14, 33–38. https://doi.org/10.1016/0263-7855(96)00018-5.

Indrakumar, S., Zalar, M., Pohl, C., Nørgaard, A., Streicher, W., Harris, P., Golovanov, A.P., Peters, G.H.J., 2019. Conformational stability study of a therapeutic peptide plectasin using molecular dynamics simulations in combination with NMR. J. Phys. Chem. B 123, 4867–4877. https://doi.org/10.1021/acs.jpcb.9b02370.

Irwin, J.J., Sterling, T., Mysinger, M.M., Bolstad, E.S., Coleman, R.G., 2012. Zinc: a free tool to discover chemistry for biology. J. Chem. Inf. Model. 52, 1757–1768. https://doi.org/10.1021/ci3001277.

Jakalian, A., Jack, D.B., Bayly, C.I., 2002. Fast, efficient generation of high-quality atomic charges. AM1-BCC model: II. Parameterization and validation. J. Comput. Chem. 23, 1623–1641. https://doi.org/10.1002/jcc.10128.

Kilár, F., Simon, I., 1985. The effect of iron binding on the conformation of transferrin. A small angle X-ray scattering study. Biophys. J. 48, 799–802. https://doi.org/10.1016/S0006-3495(85)83838-8.

Kim, S., Chen, J., Cheng, T., Gindulyte, A., He, J., He, S., Li, Q., Shoemaker, B.A., Thiessen, P.A., Yu, B., Zaslavsky, L., Zhang, J., Bolton, E.E., 2019. PubChem 2019 update: improved access to chemical data. Nucl. Acids Res. 47, D1102–D1109. https://doi.org/10.1093/nar/gky1033.

Konarev, P.V., Volkov, V.V., Sokolova, A.V., Koch, M.H.J., Svergun, D.I., 2003. PRIMUS: a Windows PC-based system for small-angle scattering data analysis. J. Appl. Crystallogr. 36, 1277–1282. https://doi.org/10.1107/S0021889803012779.

Li, P., Merz, K.M., 2014. Taking into account the ion-induced dipole interaction in the nonbonded model of ions. J. Chem. Theory Comput. 10, 289–297. https://doi.org/10.1021/ct400751u.

Lindorff-Larsen, K., Piana, S., Palmo, K., Maragakis, P., Klepeis, J.L., Dror, R.O., Shaw, D. E., 2010. Improved side-chain torsion potentials for the Amber ff99SB protein force field. Proteins Struct. Funct. Bioinforma. NA-NA. doi: 10.1002/prot.22711.

Madhavi Sastry, G., Adzhigirey, M., Day, T., Annabhimoju, R., Sherman, W., 2013. Protein and ligand preparation: parameters, protocols, and influence on virtual screening enrichments. J. Comput. Aided. Mol. Des. 27, 221–234. https://doi.org/10.1007/s10822-013-9644-8.

Maingi, V., Jain, V., Bharatam, P.V., Maiti, P.K., 2012. Dendrimer building toolkit: Model building and characterization of various dendrimer architectures. J. Comput. Chem.

33, 1997–2011. https://doi.org/10.1002/jcc.23031.
Martel, P., Kim, S.M., Powell, B.M., 1980. Physical characteristics of human transferrin from small angle neutron scattering. Biophys. J. 31, 371–380. https://doi.org/10.1016/S0006-3495(80)85065-X.
Mason, A.B., Halbrooks, P.J., James, N.G., Connolly, S.A., Larouche, J.R., Smith, V.C., MacGillivray, R.T.A., Chasteen, N.D., 2005. mutational analysis of C-lobe ligands of human serum transferrin: insights into the mechanism of iron release †. Biochemistry 44, 8013–8021. https://doi.org/10.1021/bi050015f.
Mecklenburg, S.L., Donohoe, R.J., Olah, G.A., 1997. Tertiary structural changes and iron release from human serum transferrin. J. Mol. Biol. 270, 739–750. https://doi.org/10.1006/jmbi.1997.1126.
Mongan, J., Case, D.A., McCammon, J.A., 2004. Constant pH molecular dynamics in generalized Born implicit solvent. J. Comput. Chem. 25, 2038–2048. https://doi.org/10.1002/jcc.20139.
Noinaj, N., Easley, N.C., Oke, M., Mizuno, N., Gumbart, J., Boura, E., Steere, A.N., Zak, O., Aisen, P., Tajkhorshid, E., Evans, R.W., Gorringe, A.R., Mason, A.B., Steven, A.C., Buchanan, S.K., 2012. Structural basis for iron piracy by pathogenic Neisseria. Nature. https://doi.org/10.1038/nature10823.
Panteva, M.T., Giambaşu, G.M., York, D.M., 2015. Comparison of structural, thermodynamic, kinetic and mass transport properties of Mg 2+ ion models commonly used in biomolecular simulations. J. Comput. Chem. 36, 970–982. https://doi.org/10.1002/jcc.23881.
Petoukhov, M.V., Franke, D., Shkumatov, A.V., Tria, G., Kikhney, A.G., Gajda, M., Gorba, C., Mertens, H.D.T., Konarev, P.V., Svergun, D.I., 2012. New developments in the ATSAS program package for small-angle scattering data analysis. J. Appl. Crystallogr. 45, 342–350. https://doi.org/10.1107/S0021889812007662.
Porter, J.J., Wildsmith, J., Melm, C.D., Schuchard, M.D., Ray, K.M., Chen, D.E., Scott, G.B. I., 2006. Absolute Quantification of the Lower Abundance Proteome Through Immunoaffinity Depletion of the Twenty Most Abundant Proteins in Human Serum. Sigma-Adrich Tech. Note.
Roe, D.R., Cheatham, T.E., 2013. PTRAJ and CPPTRAJ: software for processing and analysis of molecular dynamics trajectory data. J. Chem. Theory Comput. 9, 3084–3095. https://doi.org/10.1021/ct400341p.
Round, A.R., Franke, D., Moritz, S., Huchler, R., Fritsche, M., Malthan, D., Klaering, R., Svergun, D.I., Roessle, M., 2008. Automated sample-changing robot for solution scattering experiments at the EMBL Hamburg SAXS station X33. J. Appl. Crystallogr. 41, 913–917. https://doi.org/10.1107/S0021889808021018.
Shen, W., Liu, Y., Wang, H., 2019. Insulin-transferrin fusion protein and its prodrug, proinsulin-transferrin, for overcoming insulin resistance. World Pat. WO/2019/014552.
Sipe, D.M., Murphy, R.F., 1991. Binding to cellular receptors results in increased iron release from transferrin at mildly acidic pH. J. Biol. Chem. 266, 8002–16007.
Tools, D., Mirrors, S., Contact, A., 2010. ExPASy Proteomics Server. Search 1–2.
Wally, J., Halbrooks, P.J., Vonrhein, C., Rould, M.A., Everse, S.J., Mason, A.B., Buchanan, S.K., 2006. The crystal structure of iron-free human serum transferrin provides insight into inter-lobe communication and receptor binding. J. Biol. Chem. 281, 24934–24944. https://doi.org/10.1074/jbc.M604592200.
Wang, B., Turner, Andrew, J., 2006. Anchored transferrin fusion protein libraries. World Pat. WO/2006/138700.
Wang, J., Wolf, R.M., Caldwell, J.W., Kollman, P.A., Case, D.A., 2004. Development and testing of a general amber force field. J. Comput. Chem. 25, 1157–1174. https://doi.org/10.1002/jcc.20035.
Wang, W., 1999. Instability, stabilization, and formulation of liquid protein pharmaceuticals. Int. J. Pharm. 185, 129–188. https://doi.org/10.1016/S0378-5173(99)00152-0.
Wishart, D.S., Knox, C., Guo, A.C., Shrivastava, S., Hassanali, M., Stothard, P., Chang, Z., Woolsey, J., 2006. DrugBank: a comprehensive resource for in appendixlico drug discovery and exploration. Nucl. Acids Res. 34, D668–D672. https://doi.org/10.1093/nar/gkj067.
Yang, N., Zhang, H., Wang, M., Hao, Q., Sun, H., 2012. Iron and bismuth bound human serum transferrin reveals a partially-opened conformation in the N-lobe. Sci. Rep. doi: 10.1038/srep00999.
Yoon, J.-H., Chang, B.-H., Kim, S.N., Jeong, I.-H., Park, K.S., Nam, K.-Y., 2018. Pharmaceutical composition comprising mutant human growth hormone protein or transferrin fusion protein thereof as effective ingredient. World Pat. WO/2018/004294.